Thermokinetic and Spectroscopic Mapping of Carbon Monoxide Adsorption on Highly Dispersed Pt/γ-Al_2O_3

Alexis Sangnier,[1,2] Eric Genty,[3] Mathilde Iachella,[4] Philippe Sautet,[4,5] Pascal Raybaud,[2] Mickaël Matrat,[1] Christophe Dujardin,[3] Céline Chizallet[2,*]

[1] IFP Energies Nouvelles – 1 et 4 avenue de Bois-Préau – 92852 Rueil-Malmaison Cedex, France ; Institut Carnot IFPEN Transports Energies

[2] IFP Energies Nouvelles – Rond-Point de l'Echangeur de Solaize – BP 3, 69360 Solaize, France

[3] Univ. Lille, Centrale Lille, CNRS, Univ. Artois, UMR 8181, UCCS – Unité de Catalyse et Chimie du Solide, F-59000 Lille, France

[4] Université de Lyon, CNRS, Laboratoire de Chimie, Ecole Normale Supérieure de Lyon, 46 allée d'Italie, 69364 Lyon cedex 07, France

[5] Chemical and Biomolecular Engineering Department, Chemistry and Biochemistry Department and CNSI, University of California Los Angeles, California 90095, United States

KEYWORDS. Density Functional Theory, Carbon monoxide adsorption, TPD, platinum subnanometric particles, AEIR.

ABSTRACT. The understanding and quantification of the CO adsorption modes and strength on ultra-dispersed platinum catalysts supported on γ-Al_2O_3 is of prominent importance for analytic and catalytic purposes. We report a multi-scale experimental (AEIR, CO-TPD) and theoretical approach to provide vibrational properties, adsorption enthalpies, and desorption behaviours. First principles calculations on $Pt_{13}(CO)_m/\gamma$-Al_2O_3 and Pt(111) surface models (using various exchange-correlation functionals) provide a complementary view to experimental approches. Adsorption enthalpies computed with the RPBE functional appeared to be compatible with AEIR results. The occupation of top sites by CO dominates the behavior of supported Pt clusters. CO coverage reaches higher values compared to Pt(111) for similar operating conditions, and considerable cluster reconstruction is observed at high coverage. First principles calculations also confirm the IR assignement related to the various adsorption modes on top and bridge sites, and demonstrate a particle size effect, lowering the frequency of linear adsorption at top sites with respect to extended Pt(111) surfaces. Finally, first principles-based micro-kinetic modeling of CO-TPD experiments shows that the adsorption strengths predicted on the small size cluster by DFT are compatible with the experimental ones. We discuss possible reasons for the experimental desorption pattern to be much broader than the computed one.

1. Introduction

The interaction of carbon monoxide with transition metals is a wide topic of interest, with respect to its various analytical and catalytic applications. Indeed, the CO stretching mode is used as a probe of the electronic properties and nature of sites of the metal itself, as measured by the strength of the Metal-Carbonyl bond.[1] Moreover, CO is transformed into valuable chemical compounds (such as in the Fischer-Tropsch and Water Gas Shift processes).[2-3] Its removal is needed in hydrogen purification[4] and pollution abatement systems.[5] For combustion engines, aftertreatment of the exhaust gas including CO is performed thanks to heterogeneous catalysis where the active phase is a noble metal such as platinum, rhodium and palladium. In the case of platinum (scope of the present work), highly dispersed active phases show different structural, spectroscopic and reactive properties compared to extended surfaces.[6-13] Characterizing the interaction of CO with platinum particles, both from qualitative (adsorption mode and site) and quantitative (interaction strength, CO coverage) standpoints is a key milestone to better control the reactivity of CO on the metal active sites.

In the present work, we aim at unraveling at the atomic level the strength of the interaction of CO with ultra-dispersed Pt/γ-Al_2O_3 catalysts, and its consequences for the structural and spectroscopic features of the CO molecules, and for the energetics of desorption. γ-Al_2O_3 is indeed a support of large prominence in heterogeneous catalysis. Its major use in industrial processes as a support for noble metal catalysis in general is explained by its high surface area and ability to hinder catalyst sintering.[14]

The interaction of CO with platinum extended surfaces has been experimentally studied for the past 30 years by various analytical techniques.[15-23] The coordination (for molecular entities) and adsorption modes (for surfaces) were defined as given in Figure 1. LEED studies[19] and vibrational analysis[17] showed that the top position is the preferred one at low coverage (below 0.33ML) on the Pt(111) surface.

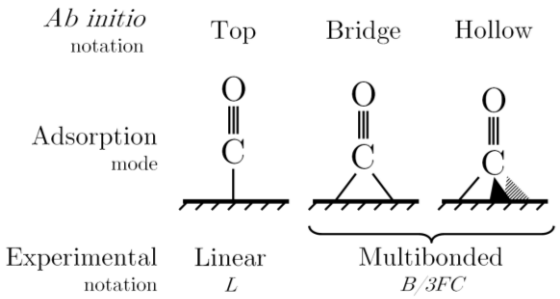

Figure 1. CO adsorption mode terminologies.

Carbon monoxide adsorbs in regular patterns that change according to the temperature, the partial pressure of CO and the surface. At higher coverage, the top and bridge positions are in competition.[18] A vibrational shift is observed for linear adsorbed CO according to the structuration of the catalyst (in particular: particle size).[24-26] In addition, the CO heats of adsorption according to several adsorption modes on Pt/Al_2O_3 were quantified via Adsorption Equilibrium InfraRed (AEIR) spectroscopy by Bianchi et al.[12,24,27-29] who investigated numerous carbonyls adsorption modes on Pt/Al_2O_3. They determined linear and multibonded heats of adsorption and demonstrated that dispersion does not significantly impact the linear species in the 0.44-0.75 dispersion range.[12,29] Pre-oxidised catalyst exhibits a peculiar 2120 cm^{-1} vibration mode[12] attributed to platinum depleted linear site (oxidised Pt^{2+}). Temperature Programmed Desorption (CO-TPD) was performed on both extended surfaces[16,20-21] and dispersed platinum supported on alumina,[30] that converge to a global desorption of CO below 500°C. Also, XAS measurements suggested that the structure of platinum particles is strongly modified upon CO adsorption.[31]

By density functional theory (DFT) calculations performed at the generalized gradient approximation (GGA) level, the preferred adsorption mode of CO on the Pt(111) surface is the hollow one, slightly more favoured than the top mode.[32-35] Yet mainly the top mode is experimentally observed.[16] Moreover, using the PBE exchange-correlation functional, adsorption energies are overestimated.[32] This contradiction named as the "CO puzzle"[33] finds its origin in an

inaccurate description of the CO HOMO-LUMO gap,[34] and is not exclusive to platinum.[32,36] The problem is solved using the Random Phase Approximation (RPA),[37] however the calculation time needed is hardly affordable. Cheaper approaches consist in applying a priori or a posteriori corrections, such as the GGA+U approach,[38] and the correlation approach using the CO singlet-triplet gap.[39-40] The role of dispersion corrections to usual functionals was also recently highlighted.[41]

Comparing CO adsorption calculated features of stepped and flat surfaces, a strong structure sensitivity was found.[42] The DFT simulations of small Pt/γ-Al_2O_3 clusters (below 1 nm) are much scarcer [43] than the one of extended surfaces or big unsupported clusters,[44-47] in particular with respect to CO adsorption properties.[48-52] However, such particles are likely to be present in oxidation catalysts. They play a key-role in alkane dehydrogenation[53] and naphta reforming catalysis.[54-55] Thus, it is crucial to compare the properties of these sub-nanometric supported particles with those of extended surfaces.

In the present work, we unravel the interaction of CO with highly dispersed Pt/γ-Al_2O_3 catalysts over a large range of CO coverage, by combining: (i) AEIR spectroscopy and CO Temperature Programmed Desorption experimental measurements, (ii) first principles calculations of the structures (including molecular dynamics), stability and vibrational feature of adsorbed CO, (iii) first principles based kinetic modelling of the CO-TPD profiles. This multi-scale approach provides unprecedented insights into the atomic scale behavior of sub-nanometric platinum particles supported on alumina in the presence of CO, accounting for the effects of CO partial pressure, and of the temperature.

2. Methods and experimental details

2.1. Sample and experimental set-ups

The catalyst (1%wt Pt/γ-Al_2O_3) was prepared by impregnation of H_2PtCl_6 solution, followed by calcination, dechlorination and reduction, as explained in a previous study.[56] X-ray fluorescence and H_2/O_2 titration on the catalyst demonstrated that almost no chlorine remains in the solid. The average particle size was estimated to be 1.07 ± 0.17 nm.[56]

Prior to the AEIR experiment, the catalyst was finely crushed and then pressed into a square pellet of 1.21 cm² (11 x 11 mm) under a pressure of 100 MPa. The mass of the final catalytic pellet was equal to 12 mg and the thickness of this wafer was estimated to 100 µm. The pellet was placed in the sample holder of a small internal volume stainless steel IR cell (0.283 cm^3) in the transmission mode described elsewhere.[57] The solid was pre-reduced *in-situ* with a controlled gas flow rate at atmospheric pressure, by the following pretreatment sequence: He (400°C, 3 hours, 10mL/min) → 5% H_2/He (400°C, 5 hours, 10mL/min) and cooling at room temperature under He flow.

The experimental procedure of the AEIR method consisted first in introducing at 25 °C a 0.3% CO/He mixture (total pressure = 1 atm, flow rate = 12 mL/min) on the catalyst. Then the temperature was slowly increased (3 °C.min^{-1}) to 400 °C while the FTIR spectra of the adsorbed species were periodically recorded (256 scans/spectrum). The AEIR procedure assumed that the evolution of a specific IR band with the increase in temperature was only due to the adsorption equilibrium, without overlap with sintering or poisoning. The recording of the adsorption was also performed during the cooling of the sample and no difference was observed with respect to the signals at ambient temperature, showing that the equilibrium coverage was reached.

The gas phase CO concentration during temperature programmed desorption (TPD) was recorded with a mass spectrometer (Pfeiffer QMS 200) on the same set-up as the AEIR experiment. The adsorption of CO was performed with a 0.3%CO/He gas mixture during one hour at 50°C. A helium flush was then applied to the catalyst during 1h at 50°C, followed by a heating ramp of 5°C.min^{-1} to gradually desorb CO, with pure helium. The total gas flow rate was kept to 12

mL.min^{-1} during the whole experiment. The mass spectrometer signals m/z=28 and 44 were recorded (respectively of CO^+ and CO_2^+ cations).

2.2. First principles calculations

The Vienna Ab initio Simulation Package (VASP[58-59]) was used for total energy and frequency calculations. A plane-wave basis set and the Projector-Augmented Wave (PAW)[60] method were employed. In a standard approach, the GGA-Perdew-Burke-Ernzerhof exchange correlation functional[61] was mainly used. We also performed some calculations using the RPBE,[62] PBE-dDsC,[63] and optPBE[64] functionals, to assess the effect of the level of theory. The cut-off energy was set to 400 eV for the plane-wave basis set and closed-shell calculations were performed. For the simulation of supported clusters, a gaussian smearing of 0.02 eV was used. The electronic optimizations were done up to a convergence of 10^{-6} eV for the self-consistent loop, and the force minimum threshold for geometry optimization was settled to 0.02 eV/Å. A dipolar correction was put in the direction perpendicular to the slab. Bader charges[65-66] were calculated at the PBE level of theory.

The model of the alumina supported platinum catalyst is composed of a 13-platinum atoms cluster on a dehydrated γ-Al_2O_3 (100) surface.[67] The diameter of the metallic particle in this model is close to 0.9 nm, in reasonable agreement with the experimental system considered in the present study. The γ-Al_2O_3(100) dehydrated surfacemodel was originally established in previous studies [68-70] and already provided important insights into the chemistry of the system.[10,43,56,67,71-74] The two platinum-layers Pt_{13} structure used in this work was found as the most stable on the (100) alumina surface.[67]

The cell parameters (16.71 x 16.79 x 30 Å^3) were chosen in order to avoid lateral interactions between periodic cluster images. Periodic slabs consist of four alumina layers (about 6 Å thickness) separated by a vacuum slab (about 24 Å thickness) corresponding to more than two

equivalent empty layers. Calculations were performed at the Γ point. We have checked that this gives energies converged up to 4.10^{-3} eV with respect to denser K-points grids. The two topmost alumina layers were relaxed, as well as platinum and adsorbate atoms, whereas the two other ones were frozen.

Non supported Pt_{13} clusters were also considered (Figure S1). The ideal Pt(111) surface was also used (Figure S2) as a reference, with five platinum layers. The dimensions of the (2x2) supercell are 8.47 x 8.47 x 29.2 $Å^3$, corresponding to a vacuum slab of 20 Å. The K-points grid was set to 5x5x1.

The adsorption energies of carbon monoxide were calculated per CO molecule, according to equation 1. The energy of CO, E_{CO}, was calculated by placing one molecule into a 15 x 15 x 15 $Å^3$ cell.

$$E_{adsorption\ CO} = \frac{1}{m}\left(E_{Pt_{13}(CO)_m} - E_{Pt_{13}} - mE_{CO}\right) \qquad \text{(Equation 1)}$$

where m is the number of CO adsorbed per cell on Pt_{13}, and E_i are the electronic energies of the corresponding systems. m describes the following values: 1, 2, 3, 6, 9, 12, 15, 18, 21 and 24 and it corresponds to the number of carbon monoxide molecules adsorbed on the Pt_{13} cluster. Energies presented in this work are displayed in $kcal.mol^{-1}$ and are computed negatively when the reaction is exothermic.

For more than one carbon monoxide adsorbed, four geometries were optimized. The most stable structure out of the four investigated in this first step was submitted to velocity-scaled molecular dynamics (MD), which proved to yield relevant results for H_2,[71,74] O_2 [56] and hydrocarbon[10] adsorptions. MD was performed with the PBE functional, at 127 °C with a time-step of 4 femtoseconds over 1200 steps, while the Pt_{13} cluster and the CO molecules were allowed to move only (the whole alumina support being frozen). In the course of the dynamics, very significant geometry changes were observed (Figure S3), even more than was observed for other adsorbates, such as hydrogen[71,74] or oxygen, [56] making us confident that we have been exploring a significant

portion of the phase space. As shown in Figure S3, the average potential energy is reaching a plateau in most of our simulations characterizing that a relevant stable configuration is found. The three most stable geometries obtained during the MD run were then chosen to be quenched by 0K geometry optimization (following the same calculation parameters as previously detailed).

The interaction energy between the alumina surface and the platinum cluster was calculated according to equation 2 using single point (*) calculations corresponding to fragments of the whole $Pt_{13}(CO)_m/\gamma\text{-}Al_2O_3$ systems.

$$E_{interaction} = \left(E_{Pt_{13}(CO)_m/\gamma-Al_2O_3} - E^*_{Pt_{13}(CO)_m} - E^*_{\gamma-Al_2O_3}\right) \qquad \text{(Equation 2)}$$

The phase diagram was built upon consideration of the most stable quenched geometries after MD. Vibrational contributions of the enthalpy and entropy were determined by harmonic frequency analysis, at the PBE level of theory. This was performed with a displacement of ±0.01 Å in each direction for all relaxed atoms in the cell. The Hessian matrix was then calculated by the finite difference method. The entropy of this condensed phase was assumed to be equal to its vibrational part neglecting rotational and translational degrees of freedom. The calculation of the free energy for each system was done similar as explained in ref. [56]. The different coverage domains represented on the thermodynamic diagrams reflects the minimum free energy among all coverages investigated. Notably, phase diagrams may also be constructed thanks to the use of alternative methods, such as Grand Canonical Monte Carlo,[75] a method that we did not explore here. The calculated adsorption enthalpies were also performed and compared to experimental heats of adsorption in the 30-500°C range.

To compare modelled and real adsorption frequencies, we computed wavelength shifts (ν_{shift}, equation 3), assuming anharmonic contributions do not differ between the gas state and the adsorbed state. Thus, simulated wavelength of vibration for adsorbed CO ($\nu_{adsorbed}$) is substracted to simulated wavelength of free CO (ν_{gas}). The same was done for experimental frequencies. We

did not apply scaling constants for the computed frequencies since we focus on frequency shift with respect to gas phase:

$$\nu_{shift} = \nu_{adsorbed} - \nu_{gas} \qquad \text{(Equation 3)}$$

2.3. Kinetic model

The Chemkin Pro ® software was used to simulate TPD experiments starting from adsorption data determined by DFT. A perfectly stirred reactor was modeled. The diffusion of gas species to the surface was not considered. The rate constants were established for both reaction directions and the temperature was settled by a temporal law simulating TPD experiments ramp.

Since the $Pt_{13}(CO)_m$ structures were investigated by varying m three-by-three, the first principles thermodynamic data were interpolated by piecewise linear patterns. The modeled mechanisms were based on molecular CO barrierless adsorption reactions following equation 4. Each direct or reverse reaction is considered up to 24 CO molecules per Pt_{13} cluster. The elemental site is one Pt_{13} particle with its global energetics.

$$Pt_{13}(CO)_m + \mathrm{CO} \rightleftarrows Pt_{13}(CO)_{m+1} \qquad \text{(Equation 4)}$$

The rate constants of molecular adsorption reactions were computed using a sticking coefficient s (set at 10^{-2}), as detailed in equation 5, with Γ_{tot} (10^{-9} cm^{-2}) the number of free sites, α the reaction order (here, 1), and M_{CO}, the molar mass of the CO molecule.

$$k_{adsorption} = \frac{s}{{\Gamma_{tot}}^{\alpha}} \sqrt{\frac{RT}{2\pi M_{\mathrm{CO}}}} \qquad \text{(Equation 5)}$$

For the reverse reaction, thermo-consistency is guaranteed by equation 6, where $\Delta_r H_{desorption}$ and $\Delta_r S_{desorption}$ stand respectively for the differential enthalpy and entropy of desorption, determined by first principles simulations between two consecutive $Pt_{13}(CO)_{m+1}$ and $Pt_{13}(CO)_m$ structures. In order to evaluate the kinetic parameter over the TPD temperature range, thermochemical parameters obtained from theoretical calculations were used to evaluate the

kinetic constant at discrete temperatures. An unconstrained nonlinear optimization was the performed using MATLAB to extract both pre-exponential factors and activation energies assuming a temperature exponent of 0.5.

$$k_{desorption} = k_{adsorption} \times exp\left(-\frac{\Delta_r H_{desorption} - T\Delta_r S_{desorption}}{RT}\right) \approx A \times \sqrt{T} \times exp\left(-\frac{E_{act}}{RT}\right)$$

(Equation 6)

Concerning the temperature, no deviation from the setpoint was observed in our experiments, implying that endothermic effects due to desorption are not significant.

3. *First principles* simulation of carbon monoxide adsorption

3.1. Adsorption of a single carbon monoxide molecule

On the supported Pt_{13} cluster, all typical adsorption sites (top, bridge and hollow sites) were set as initial guesses. Only one optimized configuration directly involves the alumina support (adsorption energy of -70 kcal.mol^{-1}) through one Al-O bond (Figure 2-a). It appears to be the most stable adsorption mode found at this CO coverage.

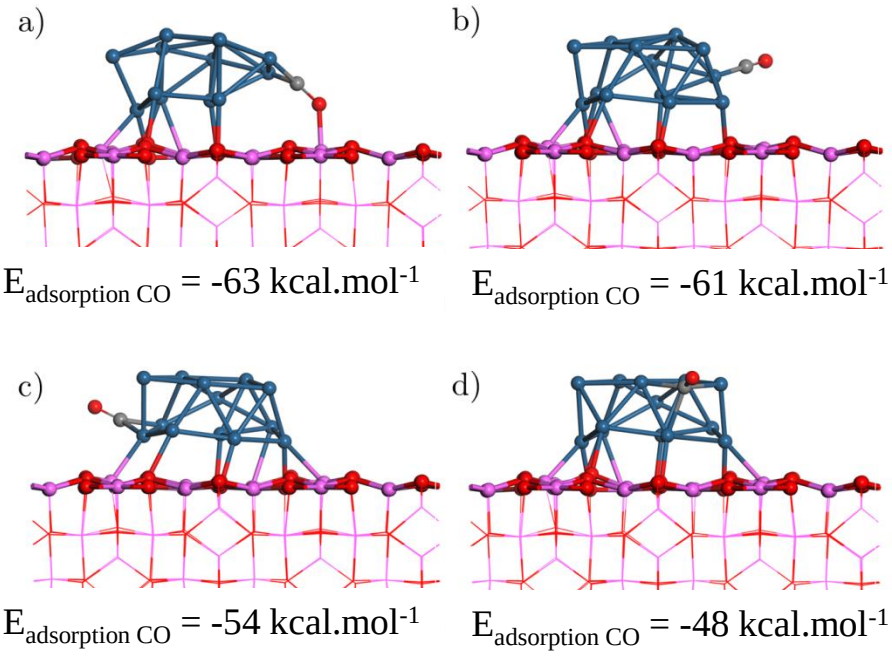

$E_{adsorption\ CO}$ = -63 kcal.mol^{-1} $E_{adsorption\ CO}$ = -61 kcal.mol^{-1}

$E_{adsorption\ CO}$ = -54 kcal.mol^{-1} $E_{adsorption\ CO}$ = -48 kcal.mol^{-1}

Figure 2. Sides views of the modes found for the adsorption of a single carbon monoxide molecule on Pt_{13}/γ-$Al_2O_3(100)$ (geometries optimized with the PBE functional, adsorption energies obtained with PBE are also reported). The a) most strongly adsorbed configuration (implying alumina) and b) top, c) bridge and d) hollow typical sites. Red: Oxygen, Purple: Aluminum, Grey: Carbon, Blue: Platinum.

Adsorption energy of CO for the most stable modes are displayed in Figure 3. Using PBE functional, the hollow site is the least stable one, compared to bridge and top sites. With the PBE dDsC, RPBE and optPBE functionals, the least stable site is the bridge site. The most stable mode , bridge sites plus interfacial Al-O bond (Figure 2-a), competes with a top adsorption mode (Figure 2-b). The comparison with extended surfaces is not straightforward due to the CO puzzle documented for Pt(111) (see introduction) and the direct or indirect role of the alumina support. The preference of the cluster for the top sites with respect to hollow sites shows that this system escapes the CO puzzle. We performed a PBE calculation on Pt(111) at 0.25ML CO coverage (Figure S2a). It exhibits an adsorption energy (-38 $kcal.mol^{-1}$) similar to the one reported by Dupont *et al.* [76] Thus, the CO adsorption energy on supported platinum cluster (-63 $kcal.mol^{-1}$) is stronger than on Pt(111) top site. Considering Pt_{38} and Pt_{55} non-supported particles,[50] a significant energy gap also appears against extended surfaces, while these clusters behave similarly to the alumina supported Pt_{13} from an energetic point of viewA non-supported Pt_{201} cluster shows weaker interaction with CO at its edge and corner (RPBE).[45]

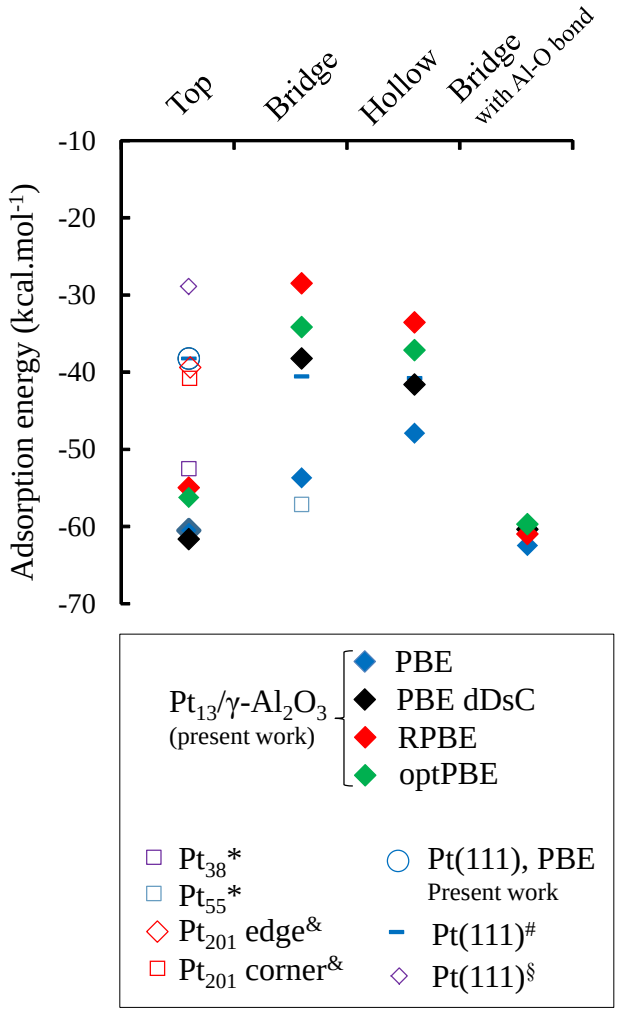

Figure 3. Adsorption energies of a single CO molecule on the supported Pt_{13} cluster (most stable adsorption configuration found for each mode), on the Pt(111) surface and on various non supported clusters from the literature. *: Johnston et al. [50] (PBE), &: Allian et al. [45] (RPBE), #: Dupont et al. [76] (PBE), §: Schimka et al. [37] (RPA).

3.2. Adsorption of CO at higher coverages

The adsorption of more than one CO was undertaken on the $Pt_{13}/\gamma\text{-}Al_2O_3$ model by MD to identify stable configurations (Figure S3). The $Pt_{13}(CO)_m/\gamma\text{-}Al_2O_3$ structures are displayed in Figure S4 with a number of CO (m) of 2, 3 and three by three up to 24. The sole adsorption mode found below 6 CO molecules is the top one with a $O-\widehat{C}-Pt$ angle close to 180°. The bridge sites appear to be occupied from $Pt_{13}(CO)_9/\gamma\text{-}Al_2O_3$ which is concomitant to the uplift of the platinum cluster. Figure 4-b displays the average distance between Pt atoms and the support (including

minimal and maximal distances). From 1 to 6 CO molecules, the average distances remain close to 0.3 nm, while the shortest and largest Pt-support distances do not strongly vary. Pt structures with 9 and 12 CO molecules exhibit similar minimal Pt-support distances as for the low coverage structures, while their average and maxima are increased by about 30%. This is typical of an uplift of the cluster as some platinum atoms are pushed upwards by the CO ligand while some Pt atoms are still hooked to the support.

This result is in line with EXAFS observations according to which the disorder increases with increasing amounts of adsorbed CO[77] (at variance with H_2, that leads to a decrease of the disorder thanks to a reconstruction into a cuboctahedron [71,74]). The average Pt-Pt distances and coordination numbers are displayed in Figure 4-c. The Pt-Pt distance strongly increases with the CO coverage, in line with a kind of a disaggregation of the cluster, a manifestation of its ductility in the presence of strongly interacting adsorbates. However, the reconstruction into a distorded cuboctahedron is favored for intermediate coverages of CO (12 and 15 molecules), whereas for higher coverages the structures is more strongly disaggregated. The 2.75-2.76 Å Pt-Pt distance measured experimentally fits well with the values obtained for 12 and 15 CO molecules per cluster. [77-79] This is accompanied by a complex evolution of the Pt-Pt coordination number. Three regimes can be described in terms of evolution of the number of undercoordinated sites: i) a first regime at low coverage ($m \leq 5$) where the coordination number of platinum slightly decreases down to 3.4, ii) a second one ($m \leq 15$) where it significantly increases up to 5.1 (for the distorted cuboctahedron), iii) a third one above $m = 15$ where it strongly decreases down to 3.4. This is a less monotonous trend than the one observed on extended surfaces[80-82] and on larger supported platinum particles,[83-84] where the under-coordinated site population continuously increases as the CO coverage increases. Actually, the cluster behaves similarly as the large particle only in the third regime. This is due to the fact that the cluster with m=15, recovers a distorted cuboctahedron morphology which is rather compact (high CN), close to the case of larger particles, and only at higher CO-coverage,

the cluster exhibits undercoordinated sites upon strong structural disaggregation. This non-monotonous behavior results from the enhanced ductility of the subnanometric clusters, that already exhibit under-coordinated sites in the absence of CO. In particular, for intermediate CO coverage (regime 2), CO induces an unexpected enhancement of the Pt-Pt CN, which cannot be observed for large Pt particles or ideal surfaces.

For the $Pt_{13}(CO)_{15}/\gamma\text{-}Al_2O_3$ structure, the minimal Pt-support distances are at least doubled. For more than 12 CO adsorbed, $Pt_{13}(CO)_m/\gamma\text{-}Al_2O_3$ displays adsorption modes with interfacial CO linked to the alumina surface (Figures S4 and S5). These interfacial species consist in four CO molecules, at 50% in the form of dimers (OC-CO, with a C-C bond) and common top/bridge modes for the remaining 50%. Notably, the simulation of non-supported $Pt_{13}(CO)_m$ clusters (Figure S1) reveals that the stability of the supported cluster is more stable than the isolated clusters plus separated support.

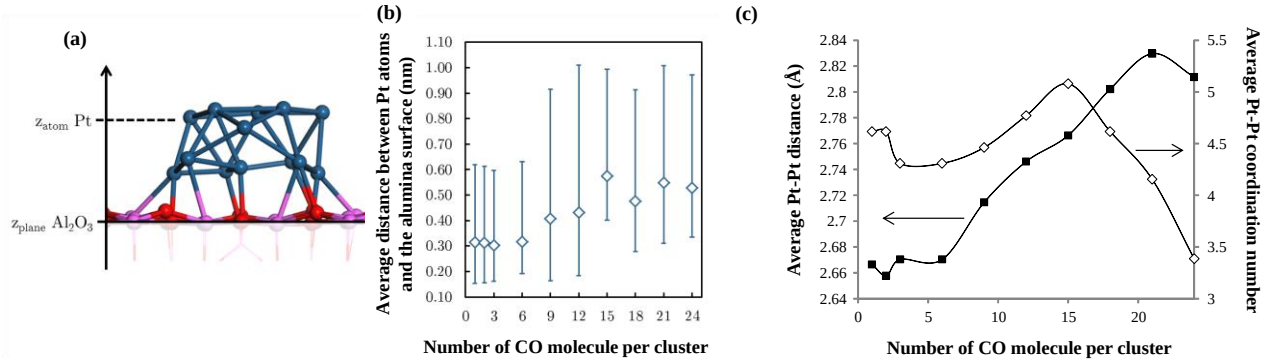

Figure 4. a) Determination of the distance of platinum atoms from the support and b) average distance between the support and the 13 platinum atoms of the cluster as a function of the number of CO molecules adsorbed per cluster. The bars correspond to minima and maxima values. c) Evolution of the average Pt-Pt distance and coordination number, for a Pt-Pt cutoff distance of 3 Å. Values obtained with the PBE functional.

This result is further confirmed by the interaction energy between the cluster and the support (Figure 5a) which is still favourable to the cluster hooking. A completely different trend happened for the cluster covered by oxygen,[56] where a strengthening of this interaction with increasing

oxygen coverage is observed. The present result is more comparable to the one obtained for the $H_2/Pt_{13}/\gamma\text{-}Al_2O_3$, H atoms leading to a disconnection of the particle from the support.[71,74] Nevertheless the adsorption modes and cluster morphology significantly differ from the one modelled upon CO adsorption.

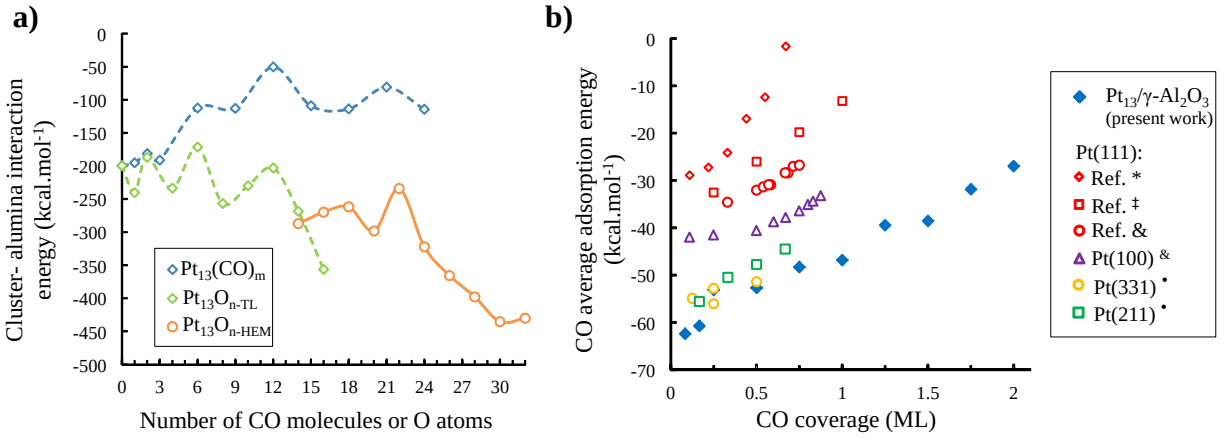

Figure 5. a) Electronic interactions between the alumina and the cluster in presence of oxygen[56] (TL: two-layer cluster, HEM: hemispherical cluster) and CO (present work, PBE functional). b) Mean adsorption energy of CO according to the carbon monoxide coverage for $Pt_{13}(CO)_m$ and Pt(111) structures, with the PBE functional. One monolayer in the present work corresponds to $Pt_{13}(CO)_{12}$ structure, as 12 platinum atoms are initially exposed at the cluster surface. The work of *Allian et al.[45] (RPBE) and coworkers, ‡Shan et al.[85] (RPBE), •Orita and Inada[86] (PBE) for stepped surfaces and &Sumaria et al.[40] (PBE with a correction using the CO singlet-triplet gap), are also reported

As shown in Figure 5b, the average adsorption energy, increases almost linearly as a function of CO coverage for highly dispersed platinum cluster, highlighting almost constant repulsion between CO molecules. The works of Allian et al.[45] and Shan et al. [85] on Pt(111) (RPBE) revealed completely different values of adsorption energies, weaker by at least 50%. The values for stepped Pt(331) and Pt(211) surfaces[86] are quite similar to the ones on supported clusters at low CO coverages.

The effect of the functional was evaluated by comparing the adsorption enthalpy using the PBE, RPBE, PBE-dDsC or opt-PBE functionals (Figure 6). Consistent with the observation of Hammer et al. on various metallic surfaces,[62] the CO adsorption enthalpy is lowered (in absolute value) with RPBE with respect to PBE. The reverse trend is most of the time observed for the

PBE-dDsC functional, also in agreement with previous calculations dealing with Pt(111).[87] Opt-PBE predicts adsorption enthalpies higher or lower than PBE, depending on the coverage, which suggests a coverage dependent nature (attractive *versus* repulsive) of dispersion interactions. The relevance of these computed values will be further discussed in section 5.1., upon comparison with AIER experimental results.

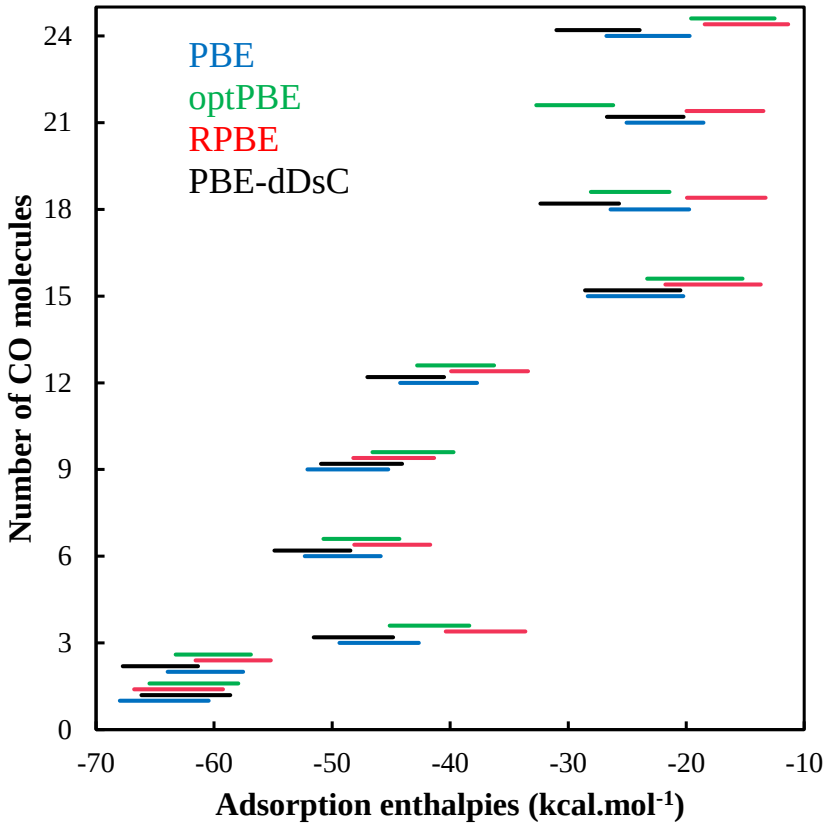

Figure 6. Evolution of the incremental adsorption enthalpy of CO with respect to the exchange-correlation functional. The lines depict the interval of adsorption enthalpies in the 30-500°C range.

Thermodynamic diagrams were then built to elucidate the dependence of the coverage on temperature and CO partial pressure. The diagram computed with the PBE functional energies and frequencies is shown in Figure 7, whereas the diagrams obtained with the three other functionals are reported in Figure S6. With all functionals, a wide domain corresponds to the clean Pt_{13} supported clusters, starting at 400°C for $P_{CO} = 10^{-4}$ bar. CO coverage increases gradually up to the most covered $Pt_{13}(CO)_{24}$ structure. As expected, the functionals accounting for the dispersion

interactions (Figure S6) shift the desorption frontiers to higher temperatures and lower CO partial pressures.

In the experimental literature, chemisorption data usually consist in the measurement of adsorption isotherms after reduction of the sample, leading to an estimation of the total amount of adsorbed CO. Then, the samples are evacuated, and a second isotherm is recorded, assumed to correspond to weakly adsorbed CO. The difference is supposed to correspond to "strongly adsorbed" CO. Following the procedure proposed by Singh et al.,[31] where adsorption isotherms are recorded at 30°C, using PBE and RPBE functionals, we predict a saturation at 12 CO per cluster, and a remaining coverage of 9 CO per cluster upon evacuation (taking the two extreme CO pressures on the diagrams, 10^{-1} and 10^{-16} bar respectively). This means that the CO/Pt total ratio is equal to 1 (dividing by 12 accessible Pt atoms) whereas the "strongly adsorbed" carbon monoxide molecules correspond to CO/Pt = 0.75. The trend is well reproduced with respect to experiments (total and "strong" CO/Pt equal to 0.86 and 0.70 respectively), although the total amount of CO is slightly overestimated. This overestimation is possibly due to i) competition between strongly adsorbed H (still present after in situ reduction and evacuation[73]) and CO, ii) to the three by three increments used in our simulations. Note that considering the PBE-dDsC and opt-PBE results (Figure S6) induces a larger overestimation of the saturation coverage (24 and 21 CO molecules at saturation, meaning CO/Pt = 2 and 1.75, at $P_{CO} = 10^{-1}$ bar), suggesting that these functionals are not well suited for the simulation of $CO/Pt_{13}/\gamma\text{-}Al_2O_3$ systems.

A comparison can be done with the STM study of CO adsorption at high coverage on Pt(111) conducted by Longwitz et al. [88]. The measurements were performed at room temperature in a 10^{-9} to 10^{3} Torr range (~10^{-12} – 1 bar) of CO partial pressure. The extreme operating points displayed respectively 0.50 and 0.70 monolayer coverage, linearly increasing on the logarithmic pressure range. In these conditions, the Pt_{13} model exhibits respectively 0.75 to 1 ML, with a transition

close to 10^{-15} bar. This illustrates the much higher affinity of CO for the subnanometric supported particles with respect to Pt(111).

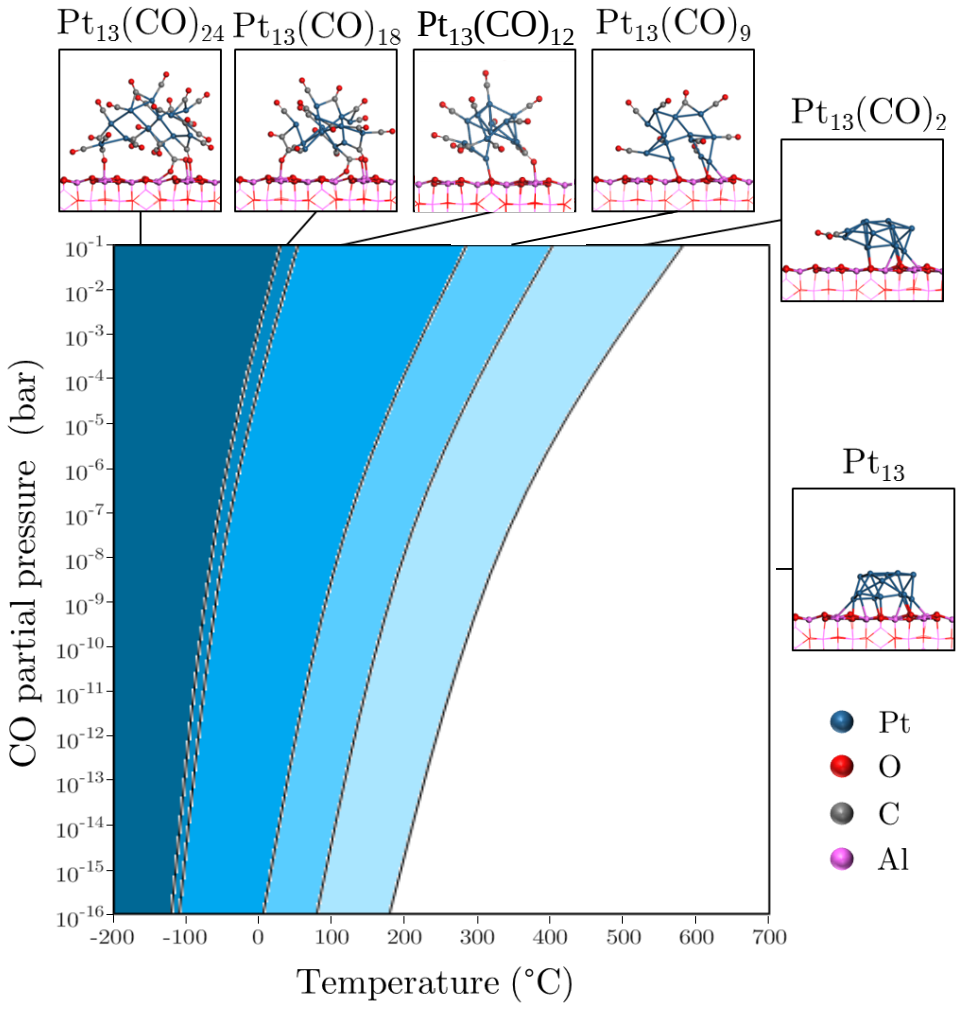

Figure 7. Phase diagram of supported $Pt_{13}(CO)_m$ structures according to temperature and partial pressure of CO, obtained with the PBE functional. The structures of the systems exhibiting a significant stability domain are also depicted (side views).

Finally, Bader charges of the cluster elements have been determined (Figure S7). No significant charge transfer between adsorbed CO to platinum is highlighted with increasing coverage, except for $Pt_{13}(CO)_1$ where the oxygen atom of CO is also connected to the support. The carbon charge is lower than the one for the isolated CO molecule, while the oxygen atom follows the opposite trend. This suggests that electrons are delocalized from O to C when CO adsorption on Pt occurs. Regarding the total charge of the adsorbed CO, a slight charge transfer from the platinum to CO

happens, because of the differences between donation and back-donation effects. Indeed, the average charge of platinum atoms becomes slightly positive (whereas it is slightly negative without CO). This can also be correlated to the preferred top site (versus bridge sites).[89] This phenomenon contrasts with the case of H_2 adsorption where the Pt cluster evolves from a negative to a positive charge at high H coverages, associated to the hydride character of H atoms.[71]

4. Determination of experimental CO vibration frequencies and heats of adsorption

4.1. IR spectra of adsorbed CO species

To experimentally evaluate the reactivity of a highly dispersed platinum catalyst supported on alumina, the determination of CO vibration frequencies and heats of adsorption (corresponding to the adsorption enthalpy) by the AEIR method have been performed. In the corresponding experimental literature, the naming of the adsorption mode is usually different from the one used so far in the present work, which is clarified in Figure 1.

The infrared spectra of the 1% wt Pt/Al_2O_3 material reduced *in situ* and put in contact with 0.3% CO/He gas flow at 25°C is displayed in Figure 8-a. The most intense band is observed at 2068 cm^{-1} that corresponds to linearly adsorbed (L, equivalent to top sites) carbon monoxide.[24] In addition, two other bands are noticed at 1882 and 1832 cm^{-1} attributed to multi-bounded (either bridge (B) or threefold (3FC)) CO species. According to the deconvolution shown in Figure 8-a, the peak assigned to linear carbonyls is composed of four bands at 2090, 2065, 2050 and 2020 cm^{-1}. Prior works identified 2070 cm^{-1} as adsorption on Pt steps and 2090 cm^{-1} on terraces.[90]

Infrared bands obtained for multibonded CO[91] lie at 1885 cm^{-1} and 1825 cm^{-1}. Bourane *et al.* demonstrated that increasing catalyst mass allows the decomposition this region into three

contributions with an additional band at 1800 cm^{-1}.[24,91] Notably, the weaker intensity of the IR band concerning the multibonded species compared to the linear species does not imply a lower amount of this species. Indeed the extinction absorption coefficient (ε) is different for the linear and B/3FC CO species.[26]

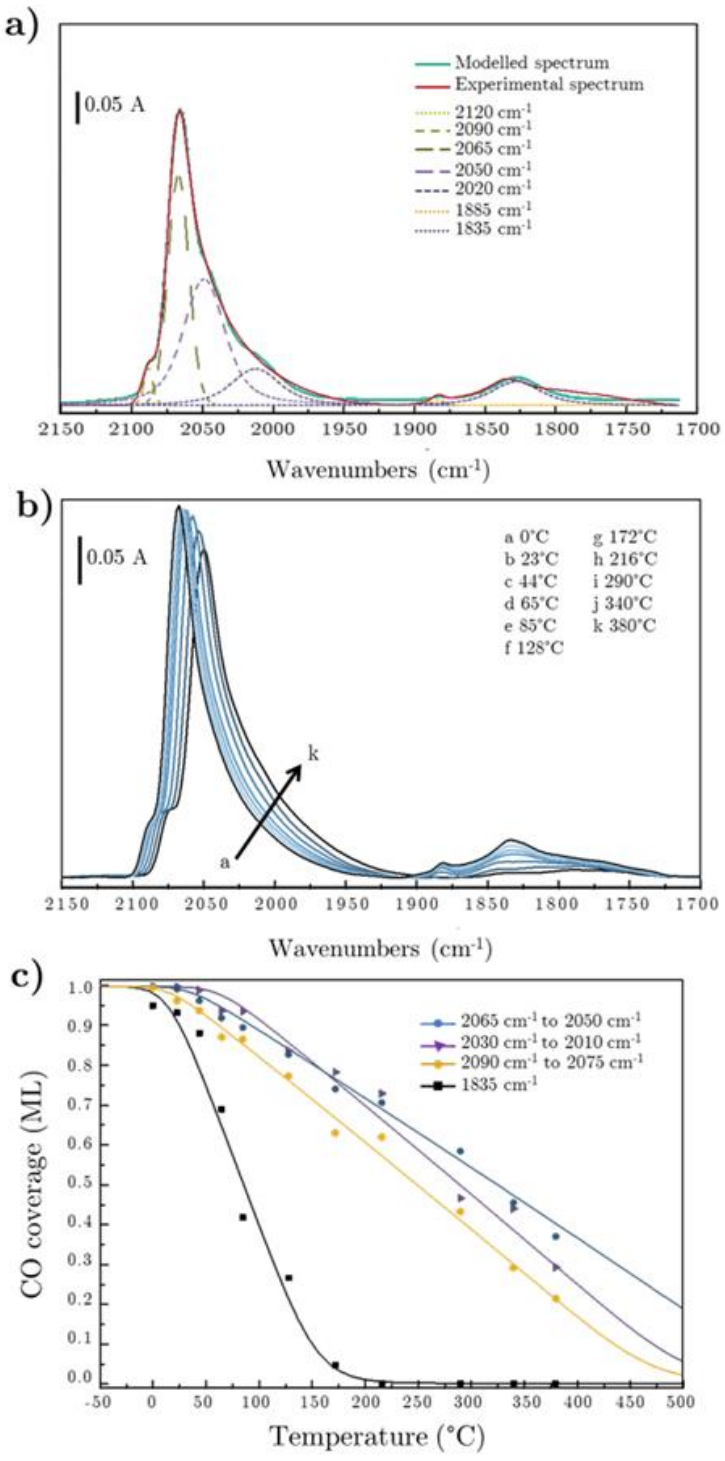

Figure 8. Adsorption Infrared Equilibrium spectrum (a) after CO adsorption at 25°C, together with the results of the spectral deconvolution, the modelled spectrum is the sum of all deconvoluted components, (b) after adsorption at various temperatures, (c) evolution of the coverage of linear and bridged CO species: comparison between experimental data (symbols) and theoretical curves (lines, Temkin adsorption model). By convention, the maximal coverage is referenced to one.

The experiment was reproduced at various temperatures (Figure 8b). The bands previously observed are shifting and their intensity changes with temperature. Considering linear species, a continuous and slow decrease of the band intensity with increasing the temperature of adsorption is observed up to 500° C. This indicates a drop of concentration of linear CO species at the catalyst surface. A slightly different behaviour is noticed for the multibonded coordinated species, which coverage rapidly reaches zero at 290°C. The observation is in accord with the work performed by Bourane et al.[91] A shift of the bands toward lower wavenumbers with increasing temperature is also visible, which can be related to the same effect observed on extended surfaces as a consequence of the decrease of the CO coverage. [92] This may also be due to the decrease of the relative intensity of the nearby 2065 cm^{-1} band.

4.2. Heat of adsorption of the linear and bridged CO species

To determine the heat of adsorption of the adsorbed CO species, the AEIR method (Adsorption Equilibrium Infrared spectroscopy method) was used.[28-29,93] This methodology is set with isobaric condition. The model assumes that the heat of adsorption decreases (in absolute value) linearly with increasing coverage. This methodology is decomposed in two steps. The first one corresponds to the determination of CO coverage (θ) for each species and at several temperatures. For the coverage determination, it is assumed that the intensity of the IR band is proportional to the concentration of this species and that temperature has no impact on the intensity. This hypothesis is considered to be acceptable, considering the good agreement of the experimental data with an adsorption model considering a linear decrease in the heat of adsorption with the coverage and

immobile adsorbed species. Thereby, the ratio between the intensity of the IR band at the temperature T_a divided by the intensity at the site saturation corresponds to the given coverage (equation 7).

$$\theta(T_a) = \frac{IR\ band\ intensity\ at\ T_a}{IR\ band\ intensity\ at\ the\ saturation\ of\ the\ sites} \quad \text{(Equation 7)}$$

The experimental coverages are reported in Figure 8c. The second step is the determination of the heat of adsorption for each species. According to the AEIR methodology, the comparison between the experimental data and the theoretical curve is performed with the generalised Temkin adsorption model (equation 8).

$$\theta = \frac{RT_a}{E_{\theta\to1} - E_{\theta\to0}}\ ln\left(\frac{1+K_{(0)}P_a}{1+K_{(1)}P_a}\right) \quad \text{(Equation 8)}$$

where $K_{(0)}$ and $K_{(1)}$ correspond to the adsorption equilibrium constants for the localized species at zero and maximum coverage respectively. $E_{\theta\to0}$ and $E_{\theta\to1}$ are the heats of adsorption for their respective CO coverage (a negative heat of adsorption corresponds to a favorable process in the present work). The adsorption equilibrium constant, K, can be estimated thanks to statistical thermodynamics and relates to the ratio of the rate constant of adsorption, and desorption of the species studied (equation 9).

$$K = \frac{h^3}{k(2\pi mk)^{3/2}}\ \frac{1}{T_a^{5/2}}\ exp\left(\frac{E_d - E_a}{RT_a}\right) \quad \text{(Equation 9)}$$

where h is the Planck's constant, k the Boltzmann's constant, m the molecular mass, T_a the adsorption temperature, E_d and E_a corresponds to the activation energies of desorption and adsorption respectively. To determine heats of adsorption at 0 and maximal coverage, a fit is performed between merged equations 8 and 9 and experimental data, with $E_{\theta\to0}$ and $E_{\theta\to1}$ the fitting parameters. The corresponding data and fitting models are reported in Figure 8-c. Related

carbon monoxide heat of adsorption are gathered in Table 1. The evolution of the intensity of the species at 1885 cm^{-1} was too low to allow us any quantification.

Table 1. Heats of adsorption determined via the AEIR method on the catalyst for each deconvoluted absorption band.

IR band			
Wavenumber	Assignment	$E_{\theta\rightarrow 0}$ ($kcal.mol^{-1}$)	$E_{\theta\rightarrow 1}$ ($kcal.mol^{-1}$)
1835 cm^{-1}	Multibonded CO	-20.3	-13.1
2030 cm^{-1}	CO(L) on Pt sub-nanometric particles	-39.4	-15.5
2065 cm^{-1}	CO(L) on Pt steps	-41.8	-14.6
2090 cm^{-1}	CO(L) on Pt terraces	-37.5	-13.1

Heats of adsorption of linear adsorption modes (2030, 2065 and 2090 cm^{-1}) lie in the same range of values with an $E_{\theta\rightarrow 0}$ around -40 $kcal.mol^{-1}$ and -14 $kcal.mol^{-1}$ at maximum coverage. These values are quite higher (in absolute value, meaning stronger interactions) than in previous works.[27,29,93-94] This difference may be due to the smaller size of Pt cluster which explains the stronger interaction with CO. Concerning the multibonded species, the heat of adsorption is lower than the ones of linear species and is similar to the literature data.[91]

5. Comparison of experimental and DFT data

5.1. At thermodynamic equilibrium

Experimental (AEIR) and computed (DFT) adsorption enthalpies are compared in Figure 9a on the 30°C-500°C temperature range, corresponding to the investigated experimental conditions. Considering the better agreement of our PBE and RPBE results with respect to chemisorption experiments (section 3.2), we mainly discuss the computational results obtained with these two functionals.

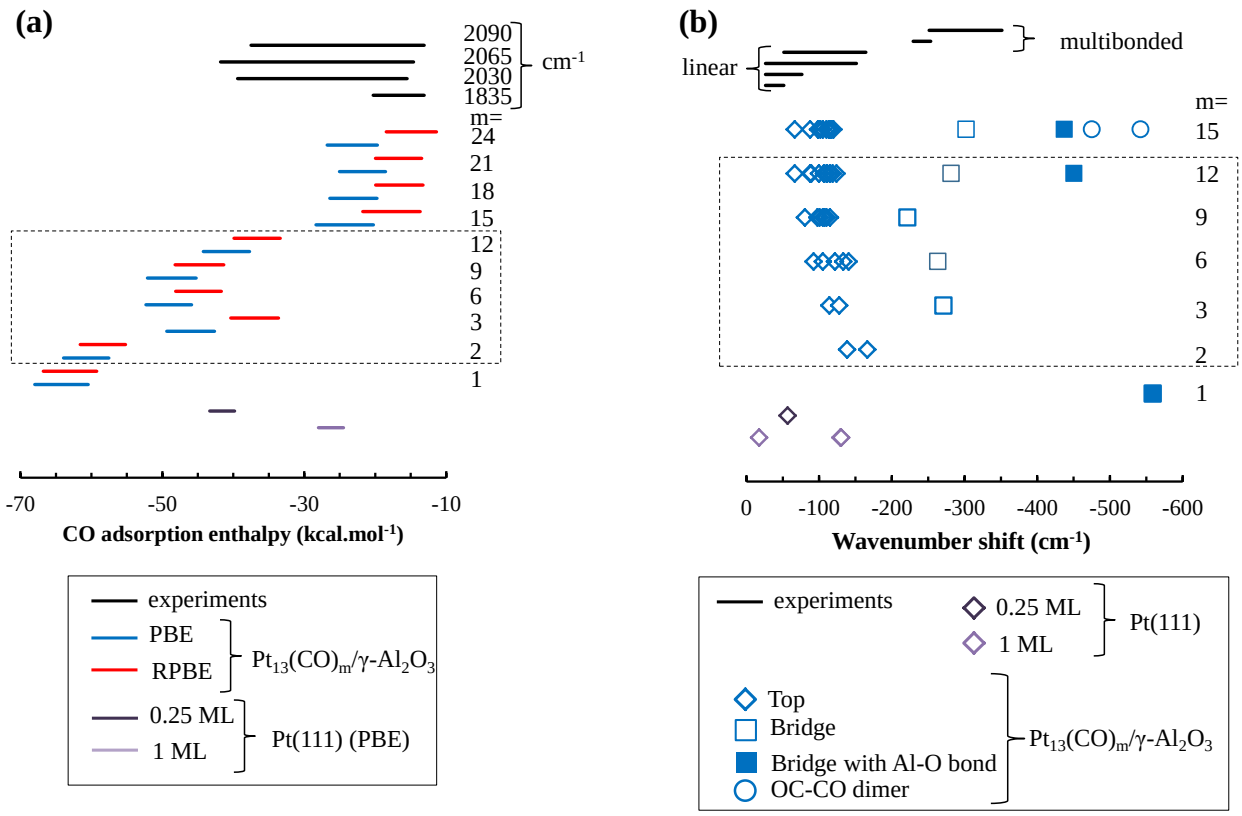

Figure 9. Experimental (AEIR) and computed (DFT) for $Pt_{13}(CO)_m$ and Pt(111): (a) CO adsorption enthalpies (experimental range: from zero coverage to maximal coverage, computed range: from 30 to 500°C); (b) CO bond vibration wavenumber shift with respect to gas phase CO, computed with the PBE exchange-correlation functional (experimental range accounts for the broadness of each deconvoluted peak). The dotted frames correspond to the m values predicted by the thermodynamic analysis.

Computed adsorption enthalpies range from -70 kcal.mol^{-1} to -20 kcal.mol^{-1} with PBE, *versus* -70 kcal.mol^{-1} to -10 kcal.mol^{-1} with RBPE. Although the computed adsorption enthalpies at low coverage are far from experimental findings, the highest CO covered structures (m≥15 with PBE, m≥3 with a few exceptions with RPBE, Figure 9) correspond to the experimental range, whatever the experimental adsorption mode. Moreover, heats of adsorption calculated on $Pt(111)_{1ML}$ are comprised between -30 and -25 kcal.mol^{-1}and do not match the experimental values. Considering $Pt(111)_{0.25ML}$, the heat of adsorption is in adequacy with low covered experimental data for the linear vibration modes. The wider interval of coverage obtained by RPBE is more compatible with the experiments. This suggests that this functional is the best compromise for the considered

system. As the PBE-dDsC and opt-PBE functionals provide even more negative adsorption enthalpies with respect to PBE, we confirm that these two functionals do not provide a satisfactory description of the interaction of CO with supported platinum clusters, compared with our AEIR experiments. Multibonded modes (bridge at most)appear mainly for $Pt_{13}(CO)_m$ with $m \geq 12$, with a population from 30 to 50% (Figure S5). That shall explain the significant difference in adsorption enthalpy with respect to lower coverages.

The comparison of experimental and computed CO vibration frequency shifts with respect to gas phase CO is given in Figure 9b. Thermodynamically, at a CO pressure close to 10^{-1} bar such as the one used experimentally, in the 0-500°C interval, RPBE calculations predict that the relevant structures are supported $Pt_{13}(CO)_m$ with $2 \leq m \leq 12$ (Figure S6-a), thus we focus on this coverage interval for the analysis of computed frequencies. m=15 was added in the series to analyze the specific vibrations due to OC-CO dimers, that appear starting from m=15. Considering the comparison between experimental linear modes and first principles top sites, all modelled wavenumbers are in the experimental range considered, except the OC-CO dimers and CO-Al species. According to our DFT calculations, the coupling of the various CO stretching modes is high. For m = 12 for example, the highest frequency mode corresponds to the symmetric vibration of all top sites (10 molecules). Thus, among the top site family for example, the relation between a given surface site and a given frequency is not straightforward.

The vibration frequency of the molecules adsorbed at the top sites increases when increasing the CO coverage (decreasing temperature), in agreement with our experiments. Moreover, the CO/Pt(111) wavenumber shifts are smaller (in absolute value) than those of CO molecules adsorbed on the supported clusters. This is in agreement with the experimental observation that linear adsorbed CO vibrations is shifted towards lower wavenumbers with decreasing size particle.[29] This shift was evaluated at 19 cm^{-1} over a dispersion range from 0.44 to 0.75, in agreement with our computational data. Bridge adsorption sites exhibit significantly lower

wavenumbers compared to top adsorption modes. CO molecules that are bridging only Pt atoms lie in the experimentally observed range for multibonded species. They are much less numerous than top sites, in agreement with the respective intensities of the signals. Bridge sites located close to the support, inducing the formation of a CO—Al bond, appear even lower in frequency, where not significant experimental detection takes place. These species are expected for m=1, 12 and 15, suggesting that the coverage is more likely to be enclosed between m=1 and 12 or 15, or that their corresponding extinction coefficients are too low to make their observation possible. OC-CO dimers are also expected at shifts lower than -400 cm^{-1}, suggesting that they are not formed in the experimental conditions under investigation. This agrees with the fact that DFT predicts their formation for $m \geq 15$ only, which is beyond that the saturation determined by DFT thermodynamics at m = 12 in the present pressure and temperature conditions. Notably, from our DFT analysis, we may not exclude m = 13 and 14 stoechiometries.

5.2. CO-TPD and micro-kinetic modelling

To go further in the comparison between DFT calculations and experimental findings, a Temperature Programmed Desorption (TPD) experiment combined with micro-kinetic modelling has been performed. The later is based on the results of the first principles calculations corresponding to supported $Pt_{13}(CO)_m$ results to determine the rate constant of desorption.

Experimental TPD (Figure 10-a) shows a 260°C desorption temperature range, from 70°C up to 330°C, with no thin distinct peak. A shoulder is visible at 70°C, followed by a steep increase of CO release with a maximum of 500 ppm at 103°C. A local maximum is reached at 144°C discerned from the first peak by a slight dip. Then a mild decrease begins up to 330°C. Notably, the desorption is complete at a lower temperature with respect to the AEIR experiment (Figure 8), which is expected considering the different atmospheres used during the thermal ramp (0.3% CO/He for AEIR, pure helium flow for TPD).

In the literature, extended surfaces show same experimental temperature ranges although a strong dependence on the initial CO coverage is observed. Considering Pt(335) stepped surface[21] and Pt(321)[20] with $0.66\theta_{max}$ initial CO coverage, CO desorbs on a wide range that covers the one of this work. Starting from $0.17\theta_{max}$, the temperature range lies from 150°C to 330°C, that corresponds to the high temperature part of our CO-TPD. The Pt(111) surface exhibits lower desorption temperatures,[16] from 50°C to 280°C. This corresponds to the low temperature range of our experiment, but this does not explain desorptions we observed at temperatures higher than 280°C. Also for similar coverages (0.5-0.66 ML), stepped surfaces[20-21] as Pt(335) and Pt(321) starts desorbing CO almost 100°C before Pt(111) surface, similarly as platinum particles. It should be noted that temperature ramp rates used in ref. [16,20-21] (10-15°C.s^{-1}) are significantly higher compared to the present work (5°C.min^{-1}). Thus, CO desorption end temperature could be overestimated. Herz and McCready[30] used a 55°C.min^{-1} heat speed on a 90% platinum dispersed catalyst supported on alumina. The major desorption appears close to 100°C, similar to our work.

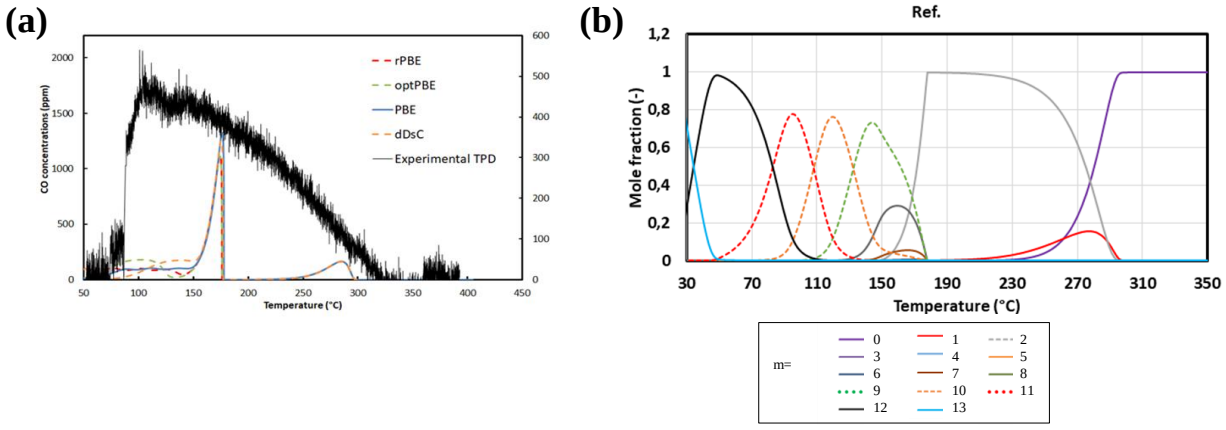

Figure 10. (a) CO-TPD simulations using various exchange functionals (colored curves, right hand size y-axis), and relative experimental intensity of CO (m/z=28, left hand size axis) during the CO-TPD on highly dispersed 1 wt. % Pt/γ-Al_2O_3 (black curve). (b) Mole fraction of each species from the simulation of the TPD, starting with the PBE DFT data.

Figure 10-a displays the TPD simulated by micro-kinetic modelling (see Table S1 for reaction parameters extracted from our first principles calculations). The modelling of the CO flow before

TPD gives the $Pt_{13}(CO)_{12}$ and $Pt_{13}(CO)_{13}$ as the dominant species. Their respective proportions depends on the functional, with the following $Pt_{13}(CO)_{12}$: $Pt_{13}(CO)_{13}$ ratio: 1:99 for PBE, 93:7 for RPBE, 9:91 for PBE-dDsC, 15:85 for optPBE. A three peaks desorption is simulated. First, a large and poorly intense peaks (or zone, depending on the functional) appears below 150°C. It corresponds to the $Pt_{13}(CO)_{12/13}$ to $Pt_{13}(CO)_9$ transition. Then, the most intense peak appears at 170°C, independently of the functional, corresponding to the $Pt_{13}(CO)_9$ to $Pt_{13}(CO)_2$ ensemble of transitions. The high temperature peak (close to 280°C) corresponds to the desorption of the two residual CO molecules from $Pt_{13}(CO)_2$. All functionals provide data that give rise to desorption peaks located in the correct interval with respect to experiments, so that their accuracy cannot be discriminated thanks to CO-TPD only. However, the computed desorption behavior is much too discrete to account for the very broad experimental feature. Thus, the shape of the signal is not reproduced. This may be explained by several origins. First, the real catalyst may not only be represented by supported Pt_{13} clusters, but a wider distribution of particle sizes contributes to the broadening. Indeed, the particle size distribution reported in ref. [56] indicates that if a majority of clusters are close to 1 nm in diameter, a few particles are bigger that the Pt_{13} model chosen here (up to 1.75 nm), while others are smaller. Moreover, the presence of single platinum atoms, that are shown to be present on similar samples thanks to high-resolution scanning electron microscopy,[95] cannot be excluded. Also, the possible role of co-adsorbed water on the particle itself (as suggested by experiments done on the Pt(111) surface[92]) needs to be further investigated. Moreover, in the present work, we only considered a single alumina facet, the dehydrated (100) one. Other facets of the alumina support are likely to contribute to the stabilization of the clusters, such as the (111) and (110) facets, that are likely to be hydroxylated in the operating conditions investigated here.[69-70,96] These hydroxyls likely influence the cluster morphology[67] and the nature of the adsorbed species on top of it.[97] Finally, the edges of the alumina platelets may also play a role on hydroxyl groups in presence, and on the stabilization of the platinum clusters.[95,98] All these

factors are likely to diversifiy the nature of the Pt sites and to enlarge the distribution of interaction strengths with CO, thus to broaden the TPD profile. Moreover, our kinetic model assumes that the sticking coefficient is kept fixed at 0.01. According to Pfnür and Menzel, [99] in the case of CO/Ru(001), the sticking coefficient may vary as (1-θ) for coverage smaller than 0.23 ($m \leq 3$ in our case) and then reaches values smaller than 0.01 for coverage greater than 0.55 ($m > 7$). To test whether this variation of the sticking coefficient as a function of the coverage has an impact or not, we evaluated the TPD profile assuming an exponential decrease of the sticking coefficient, or a linear decrease followed by exponential decrease. The impact appeared to be minor (Figure S8).

However, despite these limitations, our models provide a significant improvement in the description of the CO desorption behavior of the ultra-dispersed catalyst investigated here, with respect to the experimental knowledge obtained on Pt(111) surface, that lacks high temperature contributions.

6. Conclusion

A multi-scale experimental and theoretical approach was applied to the investigation of carbon monoxide adsorption on highly dispersed Pt/γ-Al_2O_3 catalysts. Experimentally, AEIR and CO-TPD methods provided information about the infra-red features, the adsorption enthalpies, and the desorption temperatures of CO. First principles calculations on $Pt_{13}(CO)_m$/γ-Al_2O_3 and Pt(111) surface models combined with micro-kinetic modelling of CO desorption were used to provide the same information as experimental approches. This dual approach provides unprecedented insight in the structure, vibrational properties and relevant coverage domains for the CO/Pt/γ-Al_2O_3 system. It also provides a methodological benchmark for relevant functionals to be used for the accurate theoretical description of this system. In that respect, the computation of adsorption

enthalpies compared to AEIR results, together with comparison with chemisorption results, suggests that the RPBE functional leads to the most relevant results, followed by PBE.

According to our DFT calculations, the top sites are the preferred adsorption sites for CO for highly dispersed $Pt_{13}(CO)_m$ systems supported on alumina. The adsorption energies significantly differ from the one obtained for Pt(111) flat surface, however corrugated Pt(331) and Pt(211) surfaces are quite close to dispersed $Pt_{13}(CO)_m$ data. Above one monolayer of adsorbed CO, desaggregation and uplift of the cluster happen. At the highest CO coverage, no direct Pt-alumina chemical interaction remains, and some adsorbed CO molecules intercalate between the alumina support and the platinum cluster. The exchange-correlation functional has an impact on the predicted adsorption enthalpies, as well as on the saturation coverage.

First principles calculations also confirm the IR assignement related to the various adsorption modes (top and bridge sites), and demonstrate that a particle size effect exists, lowering the frequency of linear adsorption at top sites with respect to extended Pt(111) surfaces. In the experimental conditions sampled by AEIR, the coverage varies between 0.2 and 1 ML of CO, considering the computed and experimental adsorption enthalpies, CO frequency shifts and thermodynamic phase diagrams.

Finally, computations done on the $Pt_{13}(CO)_m/\gamma\text{-}Al_2O_3$ structures allowed us to build a micro-kinetic scheme to simulate CO-TPD experiments. Simulation agrees with experimental TPD, as simulated peaks appear in the range of the experimental broad desorption. However, CO-TPD reveals a much broader desorption behavior than that predicted by the sole $Pt_{13}(CO)_m/\gamma\text{-}Al_2O_3$ models, opening perspectives for a more exhaustive simulation of the system in terms of particle size and diversity of the support model, inter alia.

Acknowledgements

This work was performed using HPC resources from GENCI-IDRIS (Grant A0020806134) and the IFPEN ENER440 supercomputer. The authors thank the Region « Hauts-de-France » and the Ministère de l'Enseignement Supérieur et de la Recherche (CPER IRENE) and the European Fund for Regional Economic Development, for their financial support.

Supporting information

Supporting_Information_Sangnier.pdf contains additional figures and table, about non supported and supported structures, phase diagrams obtained with RPBE, PBE-dDsC and opt-PBE functionals, Bader charges, kinetic modelling.

References

(1) Eischens, R. P.; Pliskin, W. A.; Francis, S. A., Infrared Spectra of Chemisorbed Carbon Monoxide, *J. Chem. Phys.* **1954**, *22*, 1786-1787.
(2) Schulz, H., Short History and Present Trends of Fischer–Tropsch Synthesis, *Appl. Catal., A* **1999**, *186*, 3-12.
(3) Grabow, L. C.; Gokhale, A. A.; Evans, S. T.; Dumesic, J. A.; Mavrikakis, M., Mechanism of the Water Gas Shift Reaction on Pt: First Principles, Experiments, and Microkinetic Modeling, *J. Phys. Chem. C* **2008**, *112*, 4608-4617.
(4) Navarro, R. M.; Peña, M. A.; Fierro, J. L. G., Hydrogen Production Reactions from Carbon Feedstocks: Fossil Fuels and Biomass, *Chem. Rev.* **2007**, *107*, 3952-3991.
(5) Russell, A.; Epling, W. S., Diesel Oxidation Catalysts, *Catal. Rev.* **2011**, *53*, 337-423.
(6) Boudart, M., Catalysis by Supported Metals, *Adv. Catal.* **1969**, *20*, 153-166.
(7) Roduner, E., Size Matters: why Nanomaterials are Different, *Chem. Soc. Rev.* **2006**, *35*, 583-592.
(8) Roldan Cuenya, B.; Behafarid, F., Nanocatalysis: Size- and Shape-Dependent Chemisorption and Catalytic Reactivity, *Surf. Sci. Rep.* **2015**, *70*, 135-187.
(9) Zhai, H.; Alexandrova, A. N., Fluxionality of Catalytic Clusters: When It Matters and How to Address It, *ACS Catal.* **2017**, *7*, 1905-1911.
(10) Zhao, W.; Chizallet, C.; Sautet, P.; Raybaud, P., Dehydrogenation Mechanisms of Methyl-Cyclohexane on γ-Al_2O_3 Supported Pt_{13}: Impact of Cluster Ductility, *J. Catal.* **2019**, *370*, 118-129.
(11) Chizallet, C.; Raybaud, P., Density Functional Theory Simulations of Complex Catalytic Materials in Reactive Environments: Beyond the Ideal Surface at Low Coverage, *Catal. Sci. Technol.* **2014**, *4*, 2797-2813.
(12) Bourane, A.; Derrouiche, S.; Bianchi, D., Impact of Pt Dispersion on the Elementary Steps of CO Oxidation by O_2 over Pt/Al_2O_3 Catalysts, *J. Catal.* **2004**, *228*, 288-297.
(13) Sun, G.; Sautet, P., Metastable Structures in Cluster Catalysis from First-Principles: Structural Ensemble in Reaction Conditions and Metastability Triggered Reactivity, *J. Am. Chem. Soc.* **2018**, *140*, 2812-2820.
(14) Euzen, P.; Raybaud, P.; Krokidis, X.; Toulhoat, H.; Loarer, J. L.; Jolivet, J.-P.; Froidefond, C.,Alumina, In *Handbook of Porous Solids*; Schüth, F., Sing, K. S. W., Weitkamp, J., Eds.; Wiley-VCH: Weinheim, 2002.

(15) Shigeishi, R. A.; King, D. A., Chemisorption of Carbon Monoxide on Platinum {111}: Reflection-Absorption Infrared Spectroscopy, *Surf. Sci.* **1976**, *58*, 379-396.
(16) Ertl, G.; Neumann, M.; Streit, K. M., Chemisorption of CO on the Pt(111) Surface, *Surf. Sci.* **1977**, *64*, 393-410.
(17) Steininger, H.; Lehwald, S.; Ibach, H., On the Adsorption of CO on Pt(111), *Surf. Sci.* **1982**, *123*, 264-282.
(18) Heyden, B. E.; Bradshaw, A. M., The Adsorption of CO on Pt(111) Studied by Infrared Reflection - Absortion Spectroscopy, *Surf. Sci.* **1983**, *125*, 787-802.
(19) Blackman, G. S.; Xu, M. L.; Ogletree, D. F.; Van Hove, M. A.; Somorjai, G. A., Mix of Molecular Adsorption Sites Detected for Disordered CO on Pt(111) by Diffuse Low-Energy Electron Diffraction, *Phys. Rev. Lett.* **1988**, *61*, 2352-2355.
(20) McClellan, M. R.; Gland, J. L.; McFeeley, F. R., Carbon Monoxide Adsorption on the Kinked Pt(321) Surface, *Surf. Sci.* **1981**, *112*, 63-77.
(21) Luo, J. S.; Tobin, R. G.; Lambert, D. K.; Fisher, G. B.; DiMaggio, C. L., CO Adsorption Site Occupation on Pt(335): a Quantitative Investigation using TPD and EELS, *Surf. Sci.* **1992**, *274*, 53-62.
(22) Greenler, R. G.; Burch, K. D.; Kretzschmar, K.; Klauser, R.; Bradshaw, A. M.; Hayden, B. E., Stepped Single-Crystal Surfaces as Models for Small Catalyst Particles, *Surf. Sci.* **1985**, *152-153*, 338-345.
(23) Hopster, H.; Ibach, H.; Comsa, G., Catalytic Oxidation of Carbon Monoxide on Stepped Platinum(111) Surfaces, *J. Catal.* **1977**, *46*, 37-48.
(24) Couble, J.; Bianchi, D., Experimental Microkinetic Approach of the CO/H_2 reaction on Pt/Al_2O_3 using the Temkin Formalism. 1. Competitive Chemisorption between Adsorbed CO and Hydrogen Species in the Absence of Reaction, *J. Catal.* **2017**, *352*, 672-685.
(25) Cybulskis, V. J.; Wang, J.; Pazmiño, J. H.; Ribeiro, F. H.; Delgass, W. N., Isotopic Transient Studies of Sodium Promotion of Pt/Al_2O_3 for the Water–Gas Shift Reaction, *J. Catal.* **2016**, *339*, 163-172.
(26) Vannice, M. A.; Twu, C. C., Extinction Coefficients and Integrated Intensities for Linear- and Bridged-Bonded CO on Platinum, *J. Chem. Phys.* **1981**, *75*, 5944-5948.
(27) Bourane, A.; Dulaurent, O.; Bianchi, D., Heats of Adsorption of the Linear CO Species Adsorbed on a Pt/Al2O3 Catalyst in the Presence of Coadsorbed Species Using FTIR Spectroscopy, *Langmuir* **2001**, *17*, 5496-5502.
(28) Bourane, A.; Dulaurent, O.; Chandes, K.; Bianchi, D., Heats of Adsorption of the Linear CO Species on a Pt/Al_2O_3 Catalyst using FTIR Spectroscopy: Comparison between TPD and Adsorption Equilibrium Procedures, *Appl. Catal. A* **2001**, *214*, 193-202.
(29) Bourane, A.; Bianchi, D., Heats of Adsorption of the Linear CO Species on Pt/Al_2O_3 using Infrared Spectroscopy: Impact of the Pt Dispersion, *J. Catal.* **2003**, *218*, 447-452.
(30) Herz, R. K.; McCready, D. F., Identification of a Weak Adsorption State of Carbon Monoxide on Highly Dispersed, Alumina-Supported Platinum, *J. Catal.* **1983**, *81*, 358-368.
(31) Singh, J.; Nelson, R. C.; Vicente, B. C.; Scott , S. L.; van Bokhoven, J. A., Electronic Structure of Alumina-Supported Monometallic Pt and Bimetallic PtSn Catalysts under Hydrogen and Carbon Monoxide Environment, *Phys. Chem. Chem. Phys.* **2010**, *12*, 5668-5677.
(32) Gajdo, M.; Eichler, A.; Hafner, J., CO Adsorption on Close-Packed Transition and Noble Metal Surfaces: Trends from ab initio Calculations, *J. Phys.: Condens. Matter* **2004**, *16*, 1141-1164.
(33) Feibelman, P. J.; Hammer, B.; Nørskov, J. K.; Wagner, F.; Scheffler, M.; Stumpf, R.; Watwe, R.; Dumesic, J., The CO/Pt(111) Puzzle, *J. Phys. Chem. B* **2001**, *105*, 4018-4025.
(34) Gil, A.; Clotet, A.; Ricart, J. M.; Kresse, G.; Garcıa-Hernández, M.; Rösch, N.; Sautet, P., Site Preference of CO Chemisorbed on Pt(111) from Density Functional Calculations, *Surf. Sci.* **2003**, *530*, 71-87.
(35) Grinberg, I.; Yourdshahyan, Y.; Rappe, A. M., CO on Pt(111) Puzzle: A Possible Solution, *J. Chem. Phys.* **2002**, *117*, 2264-2270.
(36) Hammer, B.; Morikawa, Y.; Nørskov, J. K., CO Chemisorption at Metal Surfaces and Overlayers, *Phys. Rev. Lett.* **1996**, *76*, 2141-2144.
(37) Schimka, L.; Harl, J.; Stroppa, A.; Grüneis, A.; Marsman, M.; Mittendorfer, F.; Kresse, G., Accurate Surface and Adsorption Energies from Many-Body Perturbation Theory, *Nat. Mater.* **2010**, *9*, 741-744.

(38) Kresse, G.; Gil, A.; Sautet, P., Significance of Single-Electron Energies for the Description of CO on Pt(111), *Phys. Rev. B* **2003**, *68*, 073401.
(39) Mason, S. E.; Grinberg, I.; Rappe, A. M., First-Principles Extrapolation Method for Accurate CO Adsorption Energies on Metal Surfaces, *Phys. Rev. B* **2004**, *69*, 161401.
(40) Sumaria, V.; Nguyen, L.; Tao, F. F.; Sautet, P., Optimal Packing of CO at a High Coverage on Pt(100) and Pt(111) Surfaces, *ACS Catal.* **2020**, *10*, 9533-9544.
(41) Janthon, P.; Viñes, F.; Sirijaraensre, J.; Limtrakul, J.; Illas, F., Adding Pieces to the CO/Pt(111) Puzzle: The Role of Dispersion, *J. Phys. Chem. C* **2017**, *121*, 3970-3977.
(42) Hammer, B.; Nielsen, O. H.; Norskov, J. K., Structure Sensitivity in Adsorption: CO Interaction with Stepped and Reconstructed Pt Surfaces, *Catal. Lett.* **1997**, *46*, 31-35.
(43) Raybaud, P.; Chizallet, C.; Mager-Maury, C.; Digne, M.; Toulhoat, H.; Sautet, P., From Gamma-Alumina to Supported Platinum Nanoclusters in Reforming Conditions: 10 years of DFT Modeling and Beyond, *J. Catal.* **2013**, *308*, 328-340.
(44) Dobrin, S., CO Oxidation on Pt Nanoclusters, Size and Coverage Effects: a Density Functional Theory Study, *Phys. Chem. Chem. Phys.* **2012**, *14*, 12122-12129.
(45) Allian, A. D.; Takanabe, K.; Fujdala, K. L.; Hao, X.; Truex, T. J.; Cai, J.; Buda, C.; Neurock, M.; Iglesia, E., Chemisorption of CO and Mechanism of CO Oxidation on Supported Platinum Nanoclusters, *J. Am. Chem. Soc.* **2011**, *133*, 4498-4517.
(46) Soini, T. M.; Genest, A.; Rösch, N., Assessment of Hybrid Density Functionals for the Adsorption of Carbon Monoxide on Platinum Model Clusters, *J. Phys. Chem. A* **2015**, *119*, 4051-4056.
(47) Li, L.; Larsen, A. H.; Romero, N. A.; Morozov, V. A.; Glinsvad, C.; Abild-Pedersen, F.; Greeley, J.; Jacobsen, K. W.; Norskov, J. K., Investigation of Catalytic Finite-Size-Effects of Platinum Metal Clusters, *J. Phys. Chem. Lett.* **2013**, *4*, 222-226.
(48) Yashar, Y.; Valentino, R. C.; Alexie, M. K.; Andrew, M. R., Catalytic Behavior at the Nanoscale: CO Adsorption on Al_2O_3-Supported Pt Clusters, *Proc.SPIE* **2003**, *5223*.
(49) Yin, C.; Negreiros, F. R.; Barcaro, G.; Beniya, A.; Sementa, L.; Tyo, E. C.; Bartling, S.; Meiwes-Broer, K.-H.; Seifert, S.; Hirata, H.; Isomura, N.; Nigam, S.; Majumder, C.; Watanabe, Y.; Fortunelli, A.; Vajda, S., Alumina-Supported Sub-Nanometer Pt_{10} Clusters: Amorphization and Role of the Support Material in a Highly Active CO Oxidation Catalyst, *J. Mater. Chem. A* **2017**, *5*, 4923-4931.
(50) Davis, J. B.; Baletto, F.; Johnston, R. L., The Effect of Dispersion Correction on the Adsorption of CO on Metallic Nanoparticles, *J. Phys. Chem. A* **2015**, *119*, 9703-9709.
(51) Koleva, I. Z.; Aleksandrov, H. A.; Vayssilov, G. N., Decomposition Behavior of Platinum Clusters Supported on Ceria and Gamma-Alumina in the Presence of Carbon Monoxide, *Catal. Sci. Technol.* **2017**, *7*, 734-742.
(52) Koleva, I. Z.; Aleksandrov, H. A.; Vayssilov, G. N., Influence of the adsorption of CO on the electronic structure of platinum clusters and nanowires deposited on CeO2(111) and γ-Al_2O_3(001) surfaces, *Catal. Today* **2020**, *357*, 442-452.
(53) Sattler, J. J.; Ruiz-Martinez, J.; Santillan-Jimenez, E.; Weckhuysen, B. M., Catalytic Dehydrogenation of Light Alkanes on Metals and Metal Oxides, *Chem. Rev.* **2014**, *114*, 10613-10653.
(54) Avenier, P.; Bazer-Bachi, D.; Bazer-Bachi, F.; Chizallet, C.; Deleau, F.; Diehl, F.; Gornay, J.; Lemaire, É.; Moizan-Basle, V.; Plais, C.; Raybaud, P.; Richard, F.; Lacombe, S., Catalytic Reforming: Methodology and Process Development for a Constant Optimisation and Performance Enhancement, *Oil Gas Sci. Technol. - Rev. IFPEN* **2016**, *71*, 41-59.
(55) Le Goff, P.-Y.; Kostka, W.; Ross, J.,Catalytic Reforming, In *Springer Handbook of Petroleum Technology*; Springer, Ed. 2017.
(56) Sangnier, A.; Matrat, M.; Nicolle, A.; Dujardin, C.; Chizallet, C., Multiscale Approach to the Dissociative Adsorption of Oxygen on a Highly Dispersed Platinum Supported on γ-Al_2O_3, *J. Phys. Chem. C* **2018**, *122*, 26974-26986.
(57) Legras, B.; Ordomsky, V. V.; Dujardin, C.; Virginie, M.; Khodakov, A. Y., Impact and Detailed Action of Sulfur in Syngas on Methane Synthesis on Ni/γ-Al_2O_3 Catalyst, *ACS Catal.* **2014**, *4*, 2785-2791.
(58) Kresse, G.; Hafner, J., Ab Initio Molecular-Dynamics Simulation of the Liquid-Metal-Amorphous-Semiconductor Transition in Germanium, *Phys. Rev. B* **1994**, *49*, 14251-14269.

(59) Kresse, G.; Furthmüller, J., Efficiency of Ab-Initio Total Energy Calculations for Metals and Semiconductors using a Plane-Wave Basis Set, *Comput. Mat. Sci.* **1996**, *6*, 15-50.
(60) Kresse, G.; Joubert, D., From Ultrasoft Pseudopotentials to the Projector Augmented-Wave Method, *Phys. Rev. B* **1999**, *59*, 1758-1775.
(61) Perdew, J.; Burke, K.; Ernzerhof, M., Generalized Gradient Approximation Made Simple, *Phys. Rev. Lett.* **1996**, *77*, 3865-3868.
(62) Hammer, B.; Hansen, L. B.; Nørskov, J. K., Improved Adsorption Energetics within Density-Functional Theory using Revised Perdew-Burke-Ernzerhof Functionals, *Phys. Rev. B* **1999**, *59*, 7413-7421.
(63) Steinmann, S. N.; Corminboeuf, C., Comprehensive Benchmarking of a Density-Dependent Dispersion Correction, *J Chem Theory Comput* **2011**, *7*, 3567-3577.
(64) Klimes, J.; Bowler, D. R.; Michaelides, A., Chemical Accuracy for the van der Waals Density Functional, *J. Phys.: Condens. Matter* **2010**, *22*, 022201.
(65) Sanville, E.; Kenny, S. D.; Smith, R.; Henkelman, G., Improved Grid-Based Algorithm for Bader Charge Allocation, *J. Comput. Chem.* **2007**, *28*, 899-908.
(66) Henkelman, G.; Arnaldsson, A.; Jonsson, H., A Fast and Robust Algorithm for Bader Decomposition of Charge Density, *Comput. Mat. Sci.* **2006**, *36*, 354-360.
(67) Hu, C. H.; Chizallet, C.; Mager-Maury, C.; Corral Valero, M.; Sautet, P.; Toulhoat, H.; Raybaud, P., Modulation of Catalyst Particle Structure upon Support Hydroxylation: *Ab Initio* Insights for Pd_{13} and Pt_{13} / Gamma-Al_2O_3, *J. Catal.* **2010**, *274*, 99-110.
(68) Krokidis, X.; Raybaud, P.; Gobichon, A. E.; Rebours, B.; Euzen, P.; Toulhoat, H., Theoretical Study of the Dehydration Process of Boehmite to Gamma-Alumina, *J. Phys. Chem. B* **2001**, *105*, 5121-5130.
(69) Digne, M.; Sautet, P.; Raybaud, P.; Euzen, P.; Toulhoat, H., Use of DFT to Achieve a Rational Understanding of Acid–Basic Properties of Gamma-Alumina Surfaces, *J. Catal.* **2004**, *226*, 54-68.
(70) Digne, M.; Sautet, P.; Raybaud, P.; Euzen, P.; Toulhoat, H., Hydroxyl Groups on Gamma-Alumina Surfaces: a DFT Study, *J. Catal.* **2002**, *211*, 1-5.
(71) Mager-Maury, C.; Bonnard, G.; Chizallet, C.; Sautet, P.; Raybaud, P., H_2-Induced Reconstruction of Supported Pt Clusters: Metal–Support Interaction *versus* Surface Hydride, *ChemCatChem* **2011**, *3*, 200-207.
(72) Dessal, C.; Sangnier, A.; Chizallet, C.; Dujardin, C.; Morfin, F.; Rousset, J. L.; Aouine, M.; Bugnet, M.; Afanasiev, P.; Piccolo, L., Atmosphere-Dependent Stability and Mobility of Catalytic Pt Single Atoms and Clusters on Gamma-Al_2O_3, *Nanoscale* **2019**, *11*, 6897-6904.
(73) Gorczyca, A.; Raybaud, P.; Moizan, V.; Joly, Y.; Chizallet, C., Atomistic Models for Highly-Dispersed PtSn/γ-Al_2O_3 Catalysts: Ductility and Dilution Affect the Affinity for Hydrogen, *ChemCatChem* **2019**, *11*, 3941–3951.
(74) Gorczyca, A.; Moizan, V.; Chizallet, C.; Proux, O.; Del Net, W.; Lahera, E.; Hazemann, J. L.; Raybaud, P.; Joly, Y., Monitoring Morphology and Hydrogen Coverage of Nanometric Pt/Gamma-Al_2O_3 Particles by *in situ* HERFD–XANES and Quantum Simulations, *Angew. Chem., Int. Ed.* **2014**, *53*, 12426 –12429.
(75) Liu, J. X.; Su, Y.; Filot, I. A. W.; Hensen, E. J. M., A Linear Scaling Relation for CO Oxidation on CeO_2-Supported Pd, *J. Am. Chem. Soc.* **2018**, *140*, 4580-4587.
(76) Dupont, C.; Jugnet, Y.; Loffreda, D., Theoretical Evidence of PtSn Alloy Efficiency for CO Oxidation, *J. Am. Chem. Soc.* **2006**, *128*, 9129-9136.
(77) Small, M. W.; Sanchez, S. I.; Marinkovic, N. S.; Frenkel, A. I.; Nuzzo, R. G., Influence of Adsorbates on the Electronic Structure, Bond Strain, and Thermal Properties of an Alumina-Supported Pt Catalyst, *ACS Nano* **2012**, *6*, 5583-5595.
(78) Gänzler, A. M.; Casapu, M.; Boubnov, A.; Müller, O.; Conrad, S.; Lichtenberg, H.; Frahm, R.; Grunwaldt, J.-D., Operando Spatially and Time-Resolved X-Ray Absorption Spectroscopy and Infrared Thermography During Oscillatory CO Oxidation, *J. Catal.* **2015**, *328*, 216-224.
(79) Dessal, C.; Len, T.; Morfin, F.; Rousset, J.-L.; Aouine, M.; Afanasiev, P.; Piccolo, L., Dynamics of Single Pt Atoms on Alumina during CO Oxidation Monitored by Operando X-ray and Infrared Spectroscopies, *ACS Catal.* **2019**, *9*, 5752-5759.
(80) Tao, F.; Dag, S.; Wang, L.-W.; Liu, Z.; Butcher, D. R.; Bluhm, H.; Salmeron, M.; Somorjai, G. A., Break-Up of Stepped Platinum Catalyst Surfaces by High CO Coverage, *Science* **2010**, *327*, 850.

(81) Thostrup, P.; Christoffersen, E.; Lorensen, H. T.; Jacobsen, K. W.; Besenbacher, F.; Nørskov, J. K., Adsorption-Induced Step Formation, *Phys. Rev. Lett.* **2001**, *87*, 126102.
(82) Kim, J.; Noh, M. C.; Doh, W. H.; Park, J. Y., Thermal Evolution and Instability of CO-Induced Platinum Clusters on the Pt(557) Surface at Ambient Pressure, *J. Am. Chem. Soc.* **2016**, *138*, 1110-1113.
(83) Avanesian, T.; Dai, S.; Kale, M. J.; Graham, G. W.; Pan, X.; Christopher, P., Quantitative and Atomic-Scale View of CO-Induced Pt Nanoparticle Surface Reconstruction at Saturation Coverage via DFT Calculations Coupled with in Situ TEM and IR, *J. Am. Chem. Soc.* **2017**, *139*, 4551-4558.
(84) Kale, M. J.; Christopher, P., Utilizing Quantitative in Situ FTIR Spectroscopy To Identify Well-Coordinated Pt Atoms as the Active Site for CO Oxidation on Al_2O_3-Supported Pt Catalysts, *ACS Catal.* **2016**, *6*, 5599-5609.
(85) Shan, B.; Zhao, Y.; Hyun, J.; Kapur, N.; Nicholas, J. B.; Cho, K., Coverage-Dependent CO Adsorption Energy from First-Principles Calculations, *J. Phys. Chem. C* **2009**, *113*, 6088-6092.
(86) Orita, H.; Inada, Y., DFT Investigation of CO Adsorption on Pt(211) and Pt(311) Surfaces from Low to High Coverage, *J. Phys. Chem. B* **2005**, *109*, 22469-22475.
(87) Gautier, S.; Steinmann, S. N.; Michel, C.; Fleurat-Lessard, P.; Sautet, P., Molecular Adsorption at Pt(111). How Accurate are DFT Functionals?, *Phys. Chem. Chem. Phys.* **2015**, *17*, 28921-28930
(88) Longwitz, S. R.; Schnadt, J.; Vestergaard, E. K.; Vang, R. T.; Stensgaard, I.; Brune, H.; Besenbacher, F., High-Coverage Structures of Carbon Monoxide Adsorbed on Pt(111) Studied by High-Pressure Scanning Tunneling Microscopy, *J. Phys. Chem. B* **2004**, *108*, 14497-14502.
(89) Kalhara Gunasooriya, G. T. K.; Saeys, M., CO Adsorption Site Preference on Platinum: Charge Is the Essence, *ACS Catal.* **2018**, *8*, 3770-3774.
(90) Barth, R.; Pitchai, R.; Anderson, R. L.; Verykios, X. E., Thermal Desorption-Infrared Study of Carbon Monoxide Adsorption by Alumina-Supported Platinum, *J. Catal.* **1989**, *116*, 61-70.
(91) Bourane, A.; Dulaurent, O.; Bianchi, D., Heats of Adsorption of Linear and Multibound Adsorbed CO Species on a Pt/Al_2O_3 Catalyst Using in Situ Infrared Spectroscopy under Adsorption Equilibrium, *J. Catal.* **2000**, *196*, 115-125.
(92) Rupprechter, G.; Dellwig, T.; Unterhalt, H.; Freund, H. J., High-Pressure Carbon Monoxide Adsorption on Pt(111) Revisited: A Sum Frequency Generation Study, *J. Phys. Chem. B* **2001**, *105*, 3797-3802.
(93) Bourane, A.; Bianchi, D., Oxidation of CO on a Pt/Al_2O_3 Catalyst: from the Surface Elementary Steps to Light-Off Tests: V. Experimental and Kinetic Model for Light-Off Tests in Excess of O_2, *J. Catal.* **2004**, *222*, 499-510.
(94) Jbir, I.; Paredes-Nunez, A.; Khaddar-Zine, S.; Ksibir, Z.; Meunier, F.; Bianchi, D., Heat of Adsorption of CO on EUROPT-1 Using the AEIR Method: Effect of Analysis Parameters, Water and Sample Mode, *Appl. Catal. A* **2015**, *505*, 309-318.
(95) Batista, A. T. F.; Baaziz, W.; Taleb, A.-L.; Chaniot, J.; Moreaud, M.; Legens, C.; Aguilar-Tapia, A.; Proux, O.; Hazemann, J.-L.; Diehl, F.; Chizallet, C.; Gay, A.-S.; Ersen, O.; Raybaud, P., Atomic Scale Insight into the Formation, Size, and Location of Platinum Nanoparticles Supported on γ-Alumina, *ACS Catal.* **2020**, *10*, 4193-4204.
(96) Lagauche, M.; Larmier, K.; Jolimaitre, E.; Barthelet, K.; Chizallet, C.; Favergeon, L.; Pijolat, M., Thermodynamic Characterization of the Hydroxyl Group on the γ-Alumina Surface by the Energy Distribution Function, *J. Phys. Chem. C* **2017**, *121*, 16770-16782.
(97) Mager-Maury, C.; Chizallet, C.; Sautet, P.; Raybaud, P., Platinum Nano-Clusters Stabilized on γ-alumina by Chlorine Used as a Capping Surface Ligand: a DFT Study, *ACS Catal.* **2012**, *2*, 1346-1357.
(98) Batista, A. T. F.; Wisser, D.; Pigeon, T.; Gajan, D.; Diehl, F.; Rivallan, M.; Catita, L.; Gay, A.-S.; Lesage, A.; Chizallet, C.; Raybaud, P., Beyond γ-Al_2O_3 Crystallite Surfaces: The Hidden Features of Edges Revealed by Solid-State ^{1}H NMR and DFT Calculations, *J. Catal.* **2019**, *378*, 140-143.
(99) Pfnür, H.; Menzel, D., The Influence of Adsorbate Interactions on Kinetics and Equilibrium for CO on Ru(001). I. Adsorption Kinetics, *J. Chem. Phys.* **1983**, *79*, 2400-2410.

TOC Graphic:

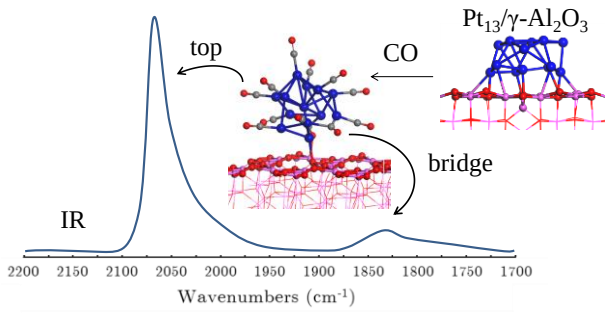
Pt13/γ-Al2O3
top
CO
bridge
IR
2200 2150 2100 2050 2000 1950 1900 1850 1800 1750 1700
Wavenumbers (cm-1)